Viscosity Dependence and Solvent Effects in the Photoisomerisation of *cis*-Stilbene: Insight from a Molecular Dynamics Study with an *ab initio* Potential Energy Function

Christian D. Berweger*, Wilfred F. van Gunsteren and Florian Müller-Plathe†

October 31, 2005

Laboratorium für Physikalische Chemie
Eidgenössische Technische Hochschule Zürich
ETH Zentrum
CH-8092 Zürich
Switzerland

† Max-Planck-Institut für Polymerforschung
Ackermannweg 10
D-55128 Mainz
Germany

* Author to whom correspondence should be addressed

For submission to: *J. Chem. Phys.*
Version: October 31, 2005

Abstract

Molecular dynamics simulations of the photoisomerisation of *cis*-stilbene in supercritical argon were performed. The stilbene molecule is represented by *ab initio* quantum chemistry, while the solvent, the interaction with solvent, and the time evolution were described by classical mechanics. Reaction rate constants are estimated and their dependence on temperature, pressure and viscosity are investigated. Good agreement with available experimental data was obtained. Our simulations strongly suggest a minimum on the excited state potential energy surface at a *gauche* conformation which is very rapidly reached after excitation, which leads to non-equilibrium barrier transitions. Specific solvent effects were identified. Implications on the current opinion on stilbene photoisomerisation are discussed.

Introduction

In the past twenty years, new developments in laser technology and in spectroscopy techniques, made it possible to observe ultrafast chemical reactions in real-time. The two most powerful and versatile techniques are fluorescence decay measurements and pump-probe spectroscopy. Their main application areas are unimolecular photoreactions, such as photo-induced dissociations or photoisomerisations. Using such techniques, it is possible to directly investigate chemical reaction dynamics on the femtosecond time scale. For example, it is possible to deduce the potential energy set free by the photodissociation of a simple molecule in gas phase [1, 2]. However, the many details of more complex systems, such as a reaction in solution, still remain unrevealed. The solvent effect in the photoisomerisation of *cis*-stilbene is dramatic: while the lifetime of an isolated excited molecule is 0.32 ps [3], in solution it ranges from 0.5 ps in methanol [4], 1.0 ps in isopentane, 1.6 ps in hexadecane [5], to 2.1 ps in cyclohexane [4]. Over many years, Jürgen Troe and his coworkers have investigated the photoisomerisation of stilbene in solution by pump-probe spectroscopy [6–11]. Still, important features of the potential energy surface are unclear and left up to speculation, and the detailed dynamics are very hard to investigate in experiment.

Nikowa et al. [7] have found that the isomerisation rate constant depends linearly on the inverse solvent viscosity. The proportionality constant A depends on the solvent type. However, Todd and Fleming [12] suggest a more general approach using molecular friction as a reference, which would be independent of the solvent. However, there is no clear definition of such a molecular friction.

Parallel to the experimental development mentioned above, a new branch of theory has evolved: computer simulation of chemical systems. It can be roughly divided into: (i) Quantum chemistry computes the electronic wave function and is capable of calculating a great variety of molecular properties at a high level of accuracy, if desired. However, it is limited to rather small molecular systems. (ii) Classical molecular dynamics uses an empirical force field and is capable of providing dynamic information of large systems at an atomic resolution. However, it is unable to simulate chemical phenomena such as bond cleavage and formation.

So why not perform molecular dynamics simulations of the photoisomerisation of stilbene? The problem is twofold. As crucial point, a force field of a photoexcited molecule is not easy to obtain. The general procedure of fitting the force field parameters to macroscopic properties of the liquid species, is not applicable. Another approach, to construct a potential energy surface suitable to reproduce selected spectroscopic data, has recently been conducted [13–16]. However, this procedure has little predictive power, since the desired results are put in previously, and then reproduced. As a last resort, one could escape to quantum chemistry. A quantum-chemical potential energy surface for stilbene [17, 18], embedded in a classical environment, seems to be a good solution. By use of an interpolation scheme, designed for the reduction of computational expense in such a situation [19, 20], such a task is indeed feasible. The results are presented in this contribution. We note that non-adiabatic quantum effects such as couplings between states have not been taken into account.

The following questions are addressed:

- What does the potential energy surface look like?
- Which trends accompany variations in temperature and in pressure?
- Can the experimental reaction rates be reproduced by our simulations?
- Is the shear viscosity as a macroscopic bulk property a good measure for the reaction rate constant as a molecular quantity?
- How can the solvent effect be described?

Methods

Computational Details

The photoreaction of *cis*-stilbene in argon solution has been simulated by means of a combined classical/quantum-mechanical model [21–23]. The solvent is described by the classical GROMOS96 [24] force field, while the potential energy surface of the reacting stilbene is obtained by *ab initio* quantum chemistry. A finite element interpolation scheme [19, 20] is used to reduce the computational expense of the quantum-chemical calculations. The method has been described in detail and the feasibility and efficiency for the same system as treated here has been demonstrated in a previous publication [20]. It is sufficient to know the following. A conformation of the molecule is fed in, and energy and gradients are returned. These quantities are calculated from an interpolated surface which is spanned by a fixed finite element grid. As soon as needed, the quantities at the grid points are calculated by *ab initio* quantum chemistry at the desired level. The results are stored for later use. Because the potential energy surface of the molecule only depends on its conformation, the same grid points can be reused through many series of simulation, also at different temperatures or pressures. This makes the method extremely efficient. However, the method requires the molecule to be constrained to a few degrees of freedom. The central ethylenic dihedral angle (labeled r_2) and the two phenyl torsional angles (r_1 and r_3) were the three degrees of freedom that spanned the potential energy surface. The other geometric parameters are optimized for the *gauche* minimum of the potential energy surface of the first excited state (S_1) of stilbene, and were constrained during the simulations. See Figure 1 and Table 1.

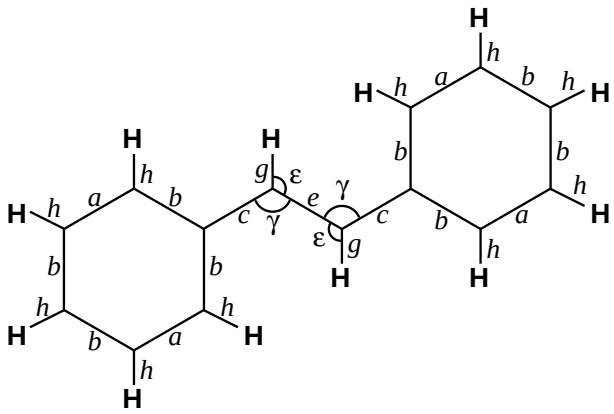

Figure 1: Geometry definition for the stilbene molecule. Geometric parameters are defined in Table 1. Bond angles that are not labeled are constrained to 120°. Phenyl rings and atoms bonded to them are held in a plane.

For the quantum chemical calculations, a configuration interaction including single excitations (CIS) in a restricted window of orbitals (from orbital number 27 to 80) has been used with the 6-31G basis set. The evaluation of the energy and the gradients with the Gaussian 94 program [25] took half an hour on average on a 440 MHz DEC Alpha processor. A higher level of theory or a larger basis set, while desirable, was still considered unaffordable. However, the potential energy surface obtained by the above-mentioned method was found to be fairly reasonable [20].

The solvent-solvent and solvent-solute interaction is modeled by standard classical force-fields. The Lennard-Jones parameters for the involved atoms were taken from the GROMOS 96 force field [24] ($\sigma_{Ar} = 0.341$ nm, $\varepsilon_{Ar} = 0.996$ kJ/mol, $\sigma_C = 0.33611$ nm, $\varepsilon_C = 0.40587$ kJ/mol, $\sigma_H = 0.23734$ nm, $\varepsilon_H = 0.11838$ kJ/mol). As combination rule for the interaction between different types of atoms, the arithmetic mean of the individual σ and the geometric mean of the individual ε are employed (Lorentz-Berthelot mixing rule).

parameter	value
a	0.13788 nm
b	0.14084 nm
c	0.14148 nm
e	0.14215 nm
g	0.10824 nm
h	0.10724 nm
γ	127.4°
ε	116.6°

Table 1: Geometry parameters for the stilbene molecule. Lowercase Latin characters indicate bond lengths, Greek characters denote bond angles.

The time step of the leap frog algorithm was 1 fs. The Lennard-Jones interaction was cut off at 0.9 nm. The temperature was weakly coupled [26] to a bath with 0.1 ps relaxation time. Geometry fixing of the stilbene molecule was achieved by distance constraints (SHAKE, [27]) with a relative tolerance of 10^{-6} and dihedral angle constraints [28] with a tolerance of 10^{-6} rad. The computational box with cubic periodic boundary conditions contained one stilbene molecule and 2744 argon atoms. Several box sizes were used for simulations at different pressures, but the volume of the box was constant during the individual simulations.

According to the Franck-Condon principle, the initial conformations of the active dihedral angles of the stilbene molecule corresponded to the *cis* minimum of the ground state (HF 6-31G**). The initial values for the free dihedral angles were 4.5° for r_2 and 43.5° for r_1 and r_3 and agree with neutron scattering experiments [29]. Initial configurations for the entire boxes were obtained by equilibrating the solvent atoms around a stilbene molecule which was held completely rigid by constraints. By using coordinates from snapshots every 1 ps in an equilibration simulation, several different starting configurations for the same state point were obtained. For the investigation of the dependence on viscosity, and some derived properties, series of simulations were performed at different temperatures and pressures.

Activation Energies

We can calculate the activation energy E_A for the reaction in an approximate way. Starting point is the Arrhenius equation,

$$k = F \exp(-E_A/k_B T) \tag{1}$$

with the pre-exponential factor F. Linearized for E_A, we obtain

$$\ln(k) = -\frac{E_A}{k_B T} + \ln F. \tag{2}$$

The reaction rate constant k is obtained from the outcome of the reaction: After a certain time interval τ, a certain ratio of the reactant molecules has already reached the final state, while the complementary ratio $s = I_a/I_0$ is still in the initial state. Assuming an exponential decay of reactants, we obtain for the reaction rate constant

$$k = -\frac{\ln I_a/I_0}{\tau}. \tag{3}$$

Insertion into Equation 2 yields

$$\ln(-\ln I_a/I_0) - \ln\tau = -\frac{E_A}{k_B T} + \ln F. \tag{4}$$

Thus, in an $\ln(-\ln s)$ vs. $-1/k_BT$ plot the activation energy E_A can be obtained from the slope of the regression line without knowing the value of τ, which only influences the intercept of the regression line.

Solvent Properties

The shear viscosity of the solvent was calculated from separate simulations of the solvent only. Simulation boxes were set up in such a way that they match the average pressures obtained from the simulations including solvent and solute. Simulation parameters were equal to the ones of the solution simulations. The pressure was sampled over 250 ps. The viscosity η was then obtained by the relation [30]

$$\eta_{\alpha\beta} = \frac{V}{k_BT}\int_0^\infty \langle \delta P_{\alpha\beta}(t)\delta P_{\alpha\beta}(0)\rangle dt \tag{5}$$

where V is the volume of the computational box, T is the temperature, and k_B is Boltzmann's constant. The integrand is the time autocorrelation function of the fluctuation of an off-diagonal element of the pressure tensor. The correlation time was obtained by fitting the numerically calculated normalized correlation function to a Lorentzian f,

$$f = \frac{1}{1+ax^2} \tag{6}$$

with the adjustable parameter a. This function has the analytical integral

$$\int_0^\infty f dx = \frac{1}{2}\frac{\pi}{\sqrt{a}} \tag{7}$$

which yields altogether

$$\eta_{\alpha\beta} = \frac{V}{2k_BT}\,\sigma^2(P_{\alpha\beta})\frac{\pi}{\sqrt{a_{\alpha\beta}}} \tag{8}$$

with $\sigma^2(P_{\alpha\beta})$ being the variance of the pressure tensor element. The viscosity η is obtained by averaging the results from the three different off-diagonal elements of the pressure tensor.

The diffusion coefficient D is calculated as

$$D = \frac{1}{6tN}\sum_i^N |\vec{x}_i - \vec{x}_i^0|^2 \tag{9}$$

with the elapsed time t after the starting configuration $\vec{x}_i^0$.

Estimation of Reaction Rate Constants

In most of the experimental work [4, 7, 8, 12, 31], an exponential decay of the signal is observed. This finding is usually attributed to an energy barrier which creates a bottleneck in the reaction pathway [7]. In this case, a small barrier is assumed near the initial *cis* region. However, as we noted in our previous work [20], no such barrier is present in our *ab initio* potential energy surface. In this subsection, we give hints how this dilemma might be resolved.

In pump-probe spectroscopy, it is generally assumed that only the conformation close to the Franck-Condon excitation region is spectroscopically visible. Nikowa et al. [7] estimate that in the case of stilbene, this small barrier is between $r_2 = 7^\circ$ and 14° for non polar solvents. With this assumption and our simulated trajectories, however, the signal would abruptly disappear after a few femtoseconds, and would not decay on a picosecond time scale as observed experimentally. If we assume, in contrast, that the spectroscopically active region is more extended, then a different picture of the photoisomerisation kinetics is possible. It might also be that the probed molecule is not in

the Franck-Condon region any more. Abrash et al. [5] find that there is no spectral shift after 100 fs which is their experimental resolution. Such a spectral shift would be likely upon conformational change. They conclude that a spectral diffusion is taking place faster than 100 fs. We will see that this interpretation is consistent with our study.

If we assume that a molecule leaves the region of spectroscopically visible conformations when it crosses the barrier between the *gauche* and the *trans* minimum, then the molecules that are caught in the *gauche* minimum remain visible, while the molecules that isomerise to the *trans* conformation disappear. The point is to find this "spectroscopic threshold". It need not be exactly at the barrier, and the exact determination is extremely difficult. Making a nonrestricive assumption, any value in the range between, say, 70° and 130° seems reasonable. Now we have indeed an energy barrier between the spectroscopically active and inactive regions. We note that this does not truly lead to an exponential decay of the signal, because the process is predominantly kinetically activated, not thermally activated. In experiment, many different effects (such as fluorescence, internal conversion, escape through a conical intersection or the photocyclisation to dihydrophenanthrene) may occur that influence the decay curve, which are not accounted for in our simulation. For simplicity, we assume that we can fit an exponential curve to our calculated data.

In an exponential decay with rate constant k, the ratio I_a/I_0 of the initial amount I_0 is still active after a time t:

$$I_a/I_0 = \exp(-kt). \tag{10}$$

From a set of simulations at a given state point, we can easily determine the ratio of molecules that remain active, as well as the average time t_T that is required to reach the spectroscopic threshold. From that, we can estimate the reaction rate constant

$$k = -\frac{\ln(I_a/I_0)}{t_T} \tag{11}$$

where I_a is the number of simulations remaining in the active region (in the *gauche* conformation in the case of stilbene) of a total number of performed simulations I_0.

Nikowa et al. [7] state that the non-radiative rate constant k_{nr} can be decomposed into the rate k_{DHP} of the photocyclisation to dihydrophenanthrene, and a viscosity dependent term with the parameter A. The parameter A is solvent-specific, but temperature-independent.

$$k_{nr} = k_{\mathrm{DHP}} + A/\eta \tag{12}$$

As the photocyclisation is not possible in the way we set up our simulation, we are left with the second term. Having calculated the rate constant k from Equation 11 and the solvent viscosity from Equation 8, we are able to calculate the A parameter

$$A = k \cdot \eta. \tag{13}$$

Results and Discussion

Potential Energy Surface

The interesting region of the potential energy surface, i. e. the regions which were at least once visited after all the simulations, is obtained as a by-product of the interpolation scheme. Table 2 gives an overview of special points on the potential energy surface, with their location and energy. So, the initial downhill energy gain is 82.4 kJ/mol, the *gauche-trans* energy barrier is 14.1 kJ/mol and the *trans-gauche* energy barrier is 11.8 kJ/mol.

Figure 2 shows a picture of the potential energy surface of stilbene in the first excited state. It shows a two-dimensional cut of the three-dimensional surface, with the condition $r_1 = r_3$ (both phenyl

Feature	Location / degree		Energy
	central dihedral	phenyl torsions	kJ/mol
cis Franck-Condon region	4.5	43.5	82.4
gauche minimum	49.8	7.9	$\stackrel{!}{=} 0$
perp barrier saddlepoint	91.6	-1.6	14.2
trans minimum	157.3	-5.1	2.3
barrier between the *trans* minima	180.0	0.0	13.5

Table 2: Selected features of the potential energy surface of the first electronically excited state of stilbene. Locations in dihedral angle space and energy are shown. The energy origin is set to zero for the *gauche* minimum.

torsion angles have the same value). Only the part of the whole surface which was known after all the simulations is shown, so virtually the space that is accessible during the photoisomerisation. The high peak in the back of the picture is the initial *cis* conformation from where the simulations were started. Figure 3 shows a top view of a symmetric cut like Figure 2. In addition, an example trajectory is shown as a white line. The coarse-grained boundary shape of the surface originates from the grid used in the interpolation scheme. Clearly visible is the *gauche* minimum and the wide, shallow 8-shaped minimum in the *trans* region, as well as the barrier in between. The top views allow easy location of the barrier. The path downhill from the starting point is very narrow, which again confirms the very low variation of the reaction trajectory in the very first phase. Also, there are steep walls on the opposite side of the *gauche* minimum. This indicates that the system is able to climb high after the rapid initial downhill motion.

The potential energy landscape looks quite different compared to previous work. While the qualitative shape is similar to most suggestions, as for example by Abrash et al. [5], Repinec et al. [32], and Saltiel [33, 34], minimum and barrier are at different dihedral angles. The minimum of the exited state is near a *gauche* conformation, while in most of the previous pictures it was assumed to be at the 90° *perp* conformation. The implications on the relaxation to the ground state would be drastic, as it is generally assumed that the relaxation occurs onto the top of the barrier separating *cis*- and *trans*-stilbene in the ground state.

Viscosity Dependence

For the investigation of the dependence on temperature and pressure, series of simulations at different state points were performed. Each series consisted of twenty individual trajectories of 5 ps, differing in the initial configuration of the solvent. For two selected pressures, three different series of twenty trajectories each were performed to obtain more data.

The trajectories of each state point were classified into categories depending upon the behaviour of the molecular system they represent: (i) the barrier is not reached, but the system is quenched to remain in the *gauche* conformation, (ii) the system crosses the barrier (the central dihedral reaches at least 92 degrees), but does not reach the *trans* minimum, but recrosses the barrier back to the *gauche* minimum, (iii) the system isomerises and relaxes to the *trans* conformation. The number of trajectories that belong to a certain category are given in Table 3 and are labeled S, R and I respectively. The boxes are labeled with ascending integer numbers for increasing pressure. A zero for simulations in vacuum will be used later. Where meaningful, an additional digit after the decimal specifies the number of the simulation series. The pressures in the simulation boxes are summarised in Table 4. Table 3 allows the following conclusions. There is a strong pressure dependence in the ratio of isomerisations. Virtually the whole range from no isomerisations to all trajectories exhibiting isomerisations is encountered. In contrast, the temperature dependence is much less pronounced. For the box labeled 5.x, there is no a clear trend in the temperature dependence, while at lower pressure (box 2.x), an

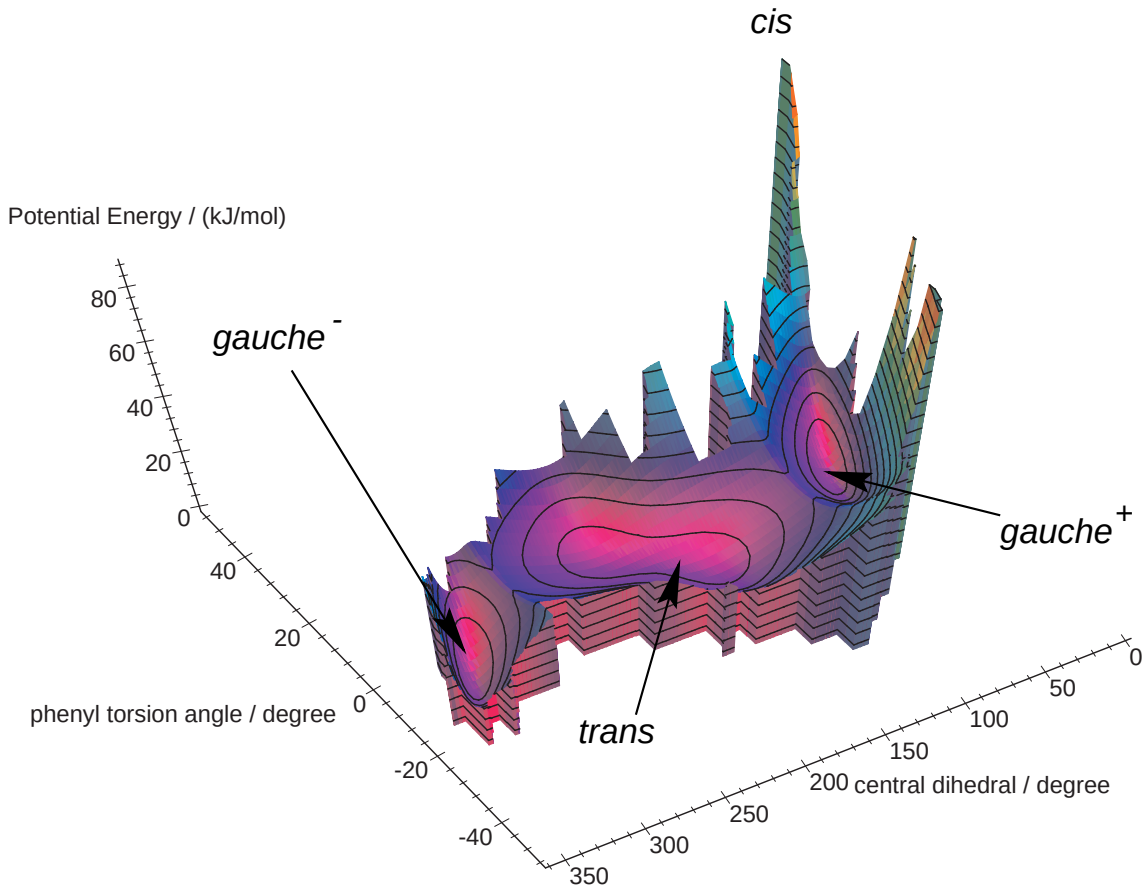

Figure 2: 3D view of the potential energy surface of the first excited state of stilbene. The picture shows a cut of the surface with both the phenyl torsion angles constrained to the same value. Only the regions that have been are visited during the simulation series are known and displayed. The distance between the contour lines is 5 kJ/mol. The high peak in the back of the figure is the *cis* Franck-Condon region from where the simulation is started. Clearly visible are the extended shallow minimum in the *trans* region, the two *gauche* minima, and the barriers in between.

increase in the ratio of isomerisations is observed with increasing temperature.

If the barrier crossing events are summarized according to the time window they occur, the picture becomes clearer. Let us call transitions that occur within the first 200 fs of the simulation kinetic activations (label K), the ones that appear later than 500 fs are thermally activated (label T). Intermediate events are labeled with M. This is done in Table 5. Again a strong pressure dependence is exhibited. More transitions are observed at low pressure. The temperature dependence is different for kinetically and thermally activated events. As one expects, more thermally activated transitions are observed at higher temperature, while the kinetic activations do not depend on temperature.

By estimating the activation energy from the ratio of isomerisations (Table 3) and by Equation 4, we obtain a value of $E_A = 4.1$ kJ/mol for the *cis-trans* isomerisation reaction. Although this value is likely to be very inaccurate, it is clearly lower than the barrier in our calculated potential energy surface. The energy difference from the *gauche* minimum to the *perp* saddlepoint is 14.1 kJ/mol. However, as will be discussed later, most of the trajectories will cross the barrier at a higher potential energy, and not at the saddlepoint. This finding would suggest that the activation energy is even higher. As this is clearly not the case, we conclude that the assumption of a thermally activated barrier crossing process is not valid. Obviously, the process is dominated by kinetic activation from the initial motion downwards from the Franck-Condon excitation region. In fact, many trajectories pass

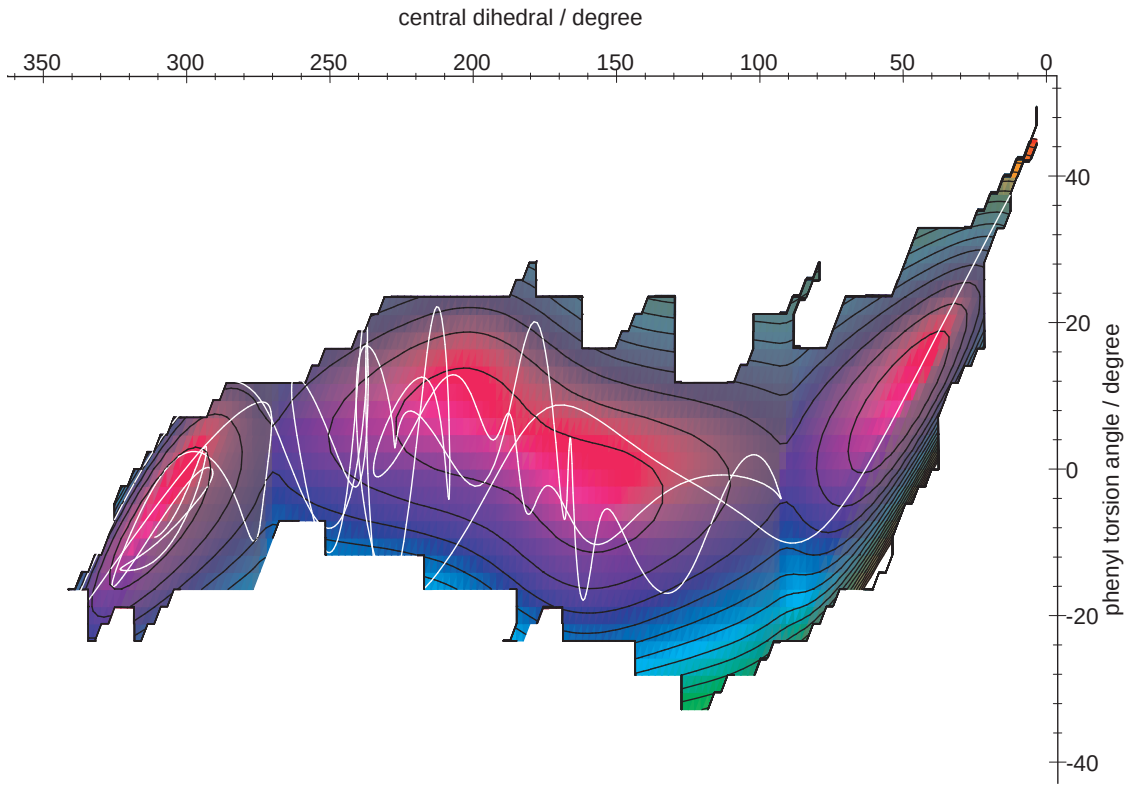

Figure 3: Top view of the potential energy surface of Figure 2. The distance between contour lines is 5 kJ/mol. A sample trajectory is drawn as a white line. It passes both barriers and ends up on the other *gauche* minimum. Note that the trajectory does not actually leave the region of the known part of the surface. This is an artifact of the representation. While the displayed surface is obtained by a symmetric cut through the real three-dimensional potential energy surface, the displayed trajectory is a projection of the real three-dimensional trajectory, i. e. one of the phenyl torsion angles is neglected.

Box	190 K			237 K			290 K			348 K		
type	S	R	I	S	R	I	S	R	I	S	R	I
1.0	2	0	18									
2.0	6	2	12	7	0	13	4	2	14	1	2	17
2.1	7	0	13	5	1	14	5	0	15	2	0	18
2.2	3	2	15	3	1	16	7	0	13	2	1	17
3.0	5	1	14	7	2	11	7	0	13	5	1	14
4.0	10	3	7	12	3	5	7	2	11	9	1	10
5.0	14	2	4	17	1	2	13	4	3	11	3	6
5.1	14	2	4	15	2	3	17	1	2	12	3	5
5.2	15	2	3	15	2	3	14	0	6	13	3	4
6.0	20	0	0	17	2	1	20	0	0	16	1	3
7.0	20	0	0									
8.0	20	0	0							19	1	0

Table 3: Classification of the trajectories of state points at four temperatures and eight box sizes for different pressures according to the behaviour of the reactions. S: stayed *gauche* R: recrossed after a barrier crossing, I: isomerised to *trans*. The box types are coded as follows. The first digit indicates the pressure: 1 is very low pressure, 8 very high pressure. The digit after the decimal indicates the serial number of a series of simulations of the same box.

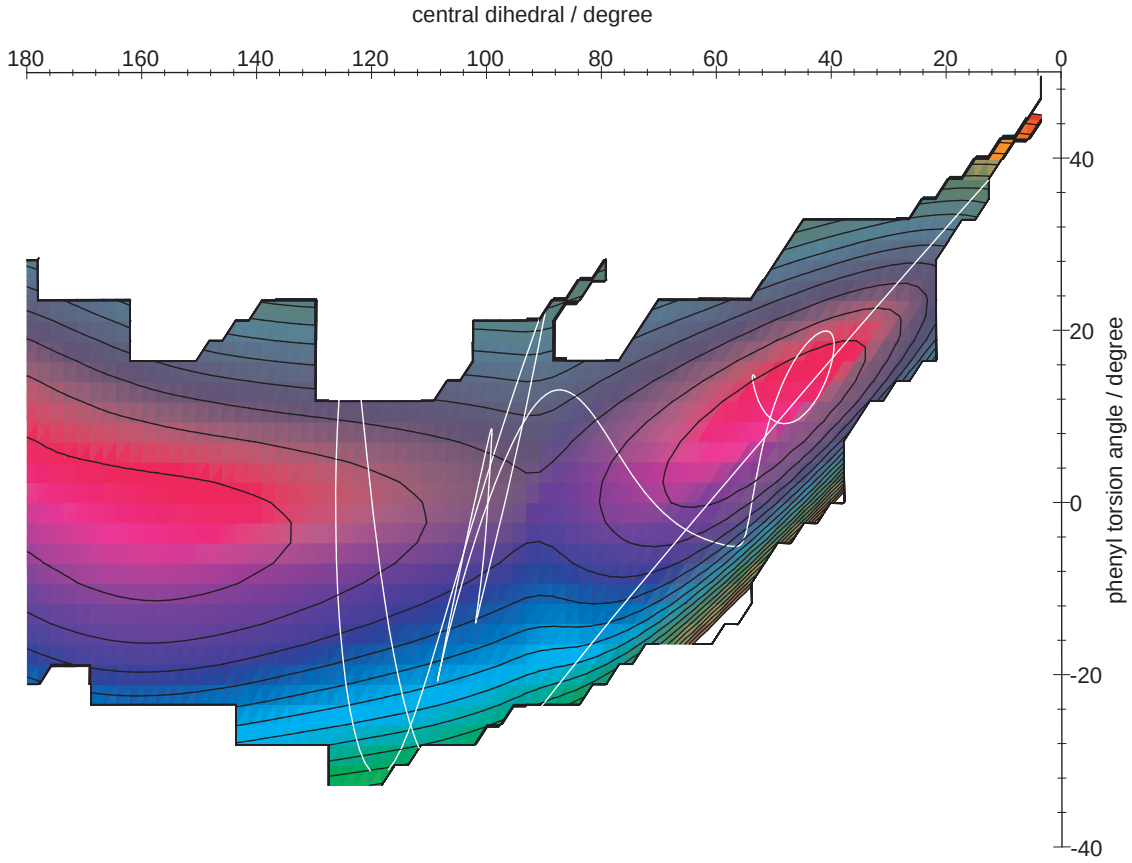

Figure 4: Top view of the potential energy surface of Figure 2. A sample trajectory is drawn as a white line. It goes actually over the barrier, but does not reach the *trans* minimum, but is reflected to the *gauche* region. See also legend for Figure 3.

Box type	solution box length / nm	solvent only simulation box length / nm	density / g cm^{-3}	reduced density
1	8.415		0.325	0.19
2	6.235	6.38	0.798	0.48
3	5.815	5.92	0.984	0.59
4	5.335	5.44	1.274	0.76
5	5.035	5.13	1.515	0.91
6	4.885	4.98	1.659	0.99
7	4.735	4.72	1.822	1.09
8	4.585		2.007	1.20

Table 4: Box sizes and density in the simulations. The density of liquid argon at 87 K and ambient pressure is 1.40 g cm^{-3} (box type 5).

Box	190 K			237 K			290 K			348 K		
type	K	M	T	K	M	T	K	M	T	K	M	T
1.0	18	0	1									
2.0	14	0	0	13	0	0	16	0	2	18	0	8
2.1	13	0	0	15	0	2	14	0	3	14	0	14
2.2	17	0	0	16	1	0	11	0	2	17	0	5
3.0	14	0	1	13	0	0	13	0	3	12	1	4
4.0	10	0	0	8	0	1	12	0	1	6	1	6
5.0	6	0	0	3	1	1	7	0	0	7	1	3
5.1	6	0	0	4	0	2	2	0	1	4	3	3
5.2	5	0	0	5	0	0	4	1	2	4	0	3
6.0	0	0	0	2	0	2	0	0	0	2	0	2
7.0	0	0	0									
8.0	0	0	0							0	0	1

Table 5: Number of barrier encounter events (the central dihedral angle reaches 92°). Kinetically activated events are shown in columns K, thermally activated events in columns T. Events that occur before 200 fs are considered to be kinetically activated, after 500 fs they contribute to columns T. The intermediate events are listed in columns M. Events may occur more than once in a single trajectory.

the *gauche* minimum in a straight line without relaxing (Figure 3). This explanation is in line with experimental results [7], which exhibit no temperature dependence of the reaction rate constants. For a thermal activation, a temperature dependence is expected for a thermal activation.

The shear viscosity of the solvent has been computed by Equations 5, 6 and 7. Results are listed in Table 6 and displayed in Figure 5. Figure 5 shows that the viscosity depends strongly on the density and thus the pressure. This effect is exploited in experiment to change the viscosity of the solvent without changing the solvent itself. On the other hand, the viscosity is basically independent of temperature. This is what is expected theoretically for a liquid at constant density.

Results for the parameter A (Equation 13) for a wide range of threshold angles reasonable in this context are given in Table 8. Experimental values for apolar solvents [7] at 295 K are: *n*-nonane 0.36 cP/ps, *n*-octane 0.32 cP/ps, *n*-hexane 0.23 cP/ps, *n*-pentane 0.16 cP/ps. Results within this range are written in bold. Experimental and computational results match quite well. A threshold angle in the range from 40° to 60° seems reasonable from the results. This coincides with the *gauche* minimum, but there need not be any causal relationship.

Table 6 shows several macroscopic properties of the solvent at the usual state points. Some of the solvent properties correlate appreciably with the rate constant. These properties are shown in Figure 6. The correlation with the self diffusion coefficient is slightly better than with the inverse viscosity. This finding suggests that the former is a better measure for the reaction rate constant. This implies that the motion of the phenyl rings is more like a particle escaping from its solvation cage than displacing a continuous medium. Looking at the Lennard-Jones sizes of the moving particles, this explanation is plausible. The diameter of an argon atom is 0.34 nm, while the diameter of a phenyl ring is 0.75 nm, and its thickness is 0.24 nm. So the sizes of the moving particles are very similar. A similar conclusion has recently been made for the self-diffusion of methanol [**?**]. However, the quality of the correlation coefficient is disputable. The next paragraph demonstrates that it is quite sensitive to small changes in the way the reaction rate is calculated.

However, the rate constant as calculated up to here consists of both kinetically and thermally activated barrier crossings. This procedure seems legitimate, as both pathways are likely to be observed in experiment. However, two objections may be raised. Firstly, the number of thermal activations is determined by the lifetime of the excited state in experiment. In our study, it depends on the simulated time span, as deactivations are not considered. Secondly, the number of thermal activations

Box type	Solvent Properties					
	ratio %	k	Viscosity	Diffusion	Pressure	Temperature
190 K						
2	67	26.20	0.005	0.0235	257.0	192.7
3	70	28.03	0.008	0.0160	418.1	190.0
4	35	9.98	0.015	0.0089	1041.5	187.6
5	18	4.68	0.027	0.0049	2448.8	189.2
6	0	0.00	0.037	0.0031	3834.1	187.6
7	0	0.00	0.024	0.0000	6431.9	190.7
237 K						
2	72	29.89	0.005	0.0268	414.4	236.2
3	55	18.59	0.008	0.0190	692.0	237.1
4	25	6.67	0.015	0.0111	1569.7	237.4
5	13	3.28	0.027	0.0065	3221.9	235.7
6	5	1.16	0.038	0.0044	4884.7	237.7
7			0.026	0.0000	7754.6	237.3
290 K						
2	70	28.32	0.005	0.0318	606.8	290.2
3	65	24.22	0.008	0.0218	991.5	290.6
4	55	18.53	0.015	0.0131	2101.2	290.4
5	18	4.80	0.025	0.0081	4051.5	289.4
6	0	0.00	0.034	0.0058	5884.4	289.3
7			0.030	0.0000	9345.1	291.4
348 K						
2	87	47.48	0.006	0.0362	821.0	350.1
3	70	28.00	0.008	0.0248	1305.3	348.4
4	50	16.01	0.016	0.0157	2652.5	348.5
5	25	6.60	0.025	0.0100	4887.6	347.0
6	15	3.66	0.035	0.0073	7000.8	351.1
7			0.068	0.0034	13781.4	349.0

Table 6: Reaction rate constants and some solvent properties. Ratio of isomerisations in percent; rate constant k (in $ps^{-}1$) estimated by Equation 3 from the 50° threshold angle. Viscosity (in cP = 10^{-3} Pa s), diffusion coefficient (in nm^2/ps), pressure (in bar) and temperature (in K) from simulations of the solvent only.

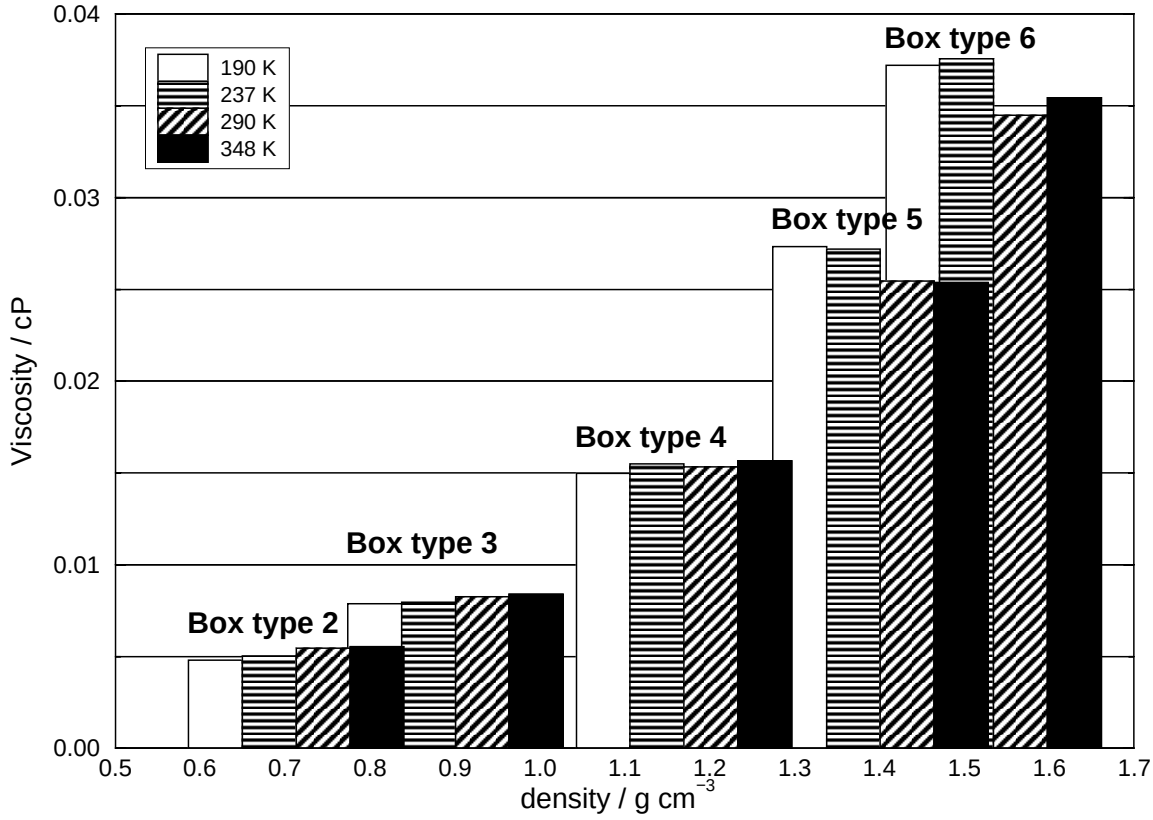

Figure 5: Shear viscosity as a function of temperature and box type (density). The viscosity is virtually independent of temperature. On the other hand, the viscosity increases remarkably with increasing density, i. e. pressure. The density of liquid argon at 87 K and ambient pressure is 1.40 g cm^{-3} (box type 5).

depend on the temperature. When applying Equation 12 in experiment, these events may be erroneously attributed to the formation of DHP, and do not enter the A parameter. If this is the case, it would make sense to consider only the kinetic activations for the parameter A_{kin}. Such results are given in Table 8 in the rightmost column and in Figure 6 in the lower row. The results do not change much, as the thermal activations are rather rare. The impact on the regression in Figure 6 is more pronounced: The correlation coefficient with the inverse viscosity reaches the same level as with the diffusion coefficient. However, it is uncertain which type of calculation is a better representation for the experiment.

Average Trajectories

Figure 7 shows trajectory averages only of isomerisations to *trans* of each state point. There is no difference between the trajectories in the first 60 fs of the simulation (Phase A). After that, a pressure dependent behaviour is observed. However, the deviations are still minor in phase B, which lasts up to 120 fs. Then the motion of the molecule is more strongly quenched, strictly with increasing pressure (phase C). This finding is clear evidence for a pressure-dependent solvent friction which damps the molecule's motion more effectively with increasing pressure. In Phase D there is a clear motion towards the *trans* minimum.

The initial motion of the dihedral angles is very rapid. After about 40 fs, the *gauche* minimum is reached. This is in good agreement with Myers and Mathies [35], which concluded from resonance Raman experiments a dihedral angle motion of 25° of the central ethylenic bond in 20 fs only. In our

Box type	Threshold angle / degrees							
	20	30	40	50	60	70	80	90
190 K								
1	127.92	91.74	69.04	53.99	42.96	34.44	28.82	23.50
2	62.08	44.59	33.56	26.20	20.75	16.71	13.34	11.04
3	66.89	47.59	35.99	28.03	22.11	17.63	14.00	11.00
4	24.00	16.99	12.78	9.98	7.85	6.16	5.06	4.12
5	11.30	8.01	6.04	4.68	3.66	2.89	2.25	1.79
6	0.00	0.00	0.00	0.00	0.00	0.00	0.00	0.00
237 K								
2	71.42	51.06	38.45	29.89	23.83	19.06	14.96	12.22
3	44.24	31.75	23.84	18.59	14.60	11.83	9.25	7.27
4	16.03	11.44	8.64	6.67	5.20	4.09	3.28	2.80
5	7.98	5.68	4.25	3.28	2.56	1.97	1.60	1.27
6	2.85	2.03	1.51	1.16	0.92	0.71	0.56	0.41
290 K								
2	67.35	48.25	36.27	28.32	22.44	17.95	14.26	11.59
3	58.00	41.41	31.24	24.22	19.19	15.21	12.59	9.97
4	44.36	31.75	23.87	18.53	14.51	11.40	9.67	7.56
5	11.59	8.25	6.19	4.80	3.79	2.91	2.29	1.92
6	0.00	0.00	0.00	0.00	0.00	0.00	0.00	0.00
348 K								
2	113.05	80.89	60.86	47.48	37.61	29.88	24.54	19.60
3	66.89	47.97	35.94	28.00	22.19	17.50	13.86	11.78
4	38.72	27.29	20.63	16.01	12.39	9.59	7.83	5.86
5	16.19	11.40	8.58	6.60	5.07	3.92	3.33	2.61
6	9.03	6.32	4.85	3.66	2.94	2.23	1.87	1.47

Table 7: Rate constants for several threshold angles, obtained from a series of simulations at the usual temperatures and box types. Estimated from Equation 11.

simulation, this dihedral angle is reached after 25 fs.

The trajectories in phase C of Figure 7 all show an interesting feature. The slope of the trajectory ($\partial r_2/\partial t$, "speed of reaction") decreases after the barrier (at 92°) has been crossed. This is in contrast to the expectation that the molecule relaxes quickly to the minimum once the barrier has been crossed. There are two reasons for the observed behaviour: (i) the phenyl rings need to rearrange before the central dihedral is able to relax, (ii) solvent friction is particularly effective in this region. The solvent effects can be investigated by comparing to the simulation of the isomerisation in vacuo. The vacuum simulation is probably a poor representation of the gas phase reaction, in which internal vibrational energy redistribution (IVR) is likely to be an important relaxation pathway, but not allowed for in the simulation. However, it is consistent with the simulations of the system in solution, in which the interaction with the solvent is assumed to be the major source of relaxation. Figure 8 shows the dihedral angle trajectories of the system in vacuo (dashed lines) in comparison to the system in solution (solid lines). Only the trajectories that exhibited isomerisation were averaged and are shown with standard deviations (thin lines). The trajectories originate from simulations at 190 K in a box of 5.035 nm each edge, which corresponds to the highest pressure of a system in which isomerisations still occurred. The phenyl ring torsion angles are also shown. Trajectories in both vacuum and solvent show that during the flattened phase of the central dihedral angle (between 100 and 250 fs) the motion of the phenyl torsion angles is reversed. Figure 10 shows a peak in the solvent-solute interaction potential energy at 250 fs, exactly the time when the dihedral angles in Figure 8 do not change much.

The dot-dashed line in Figure 8 represents the angle between the plane of the two phenyl rings. This angle may serve as a measure of impact of the reaction on the solvent. One can see that in

Box type	parameter $A = \eta/t_T$ [cP/ps]								
	Threshold angle / degrees								A_{kin}
	20	30	40	50	60	70	80	90	50
190 K									
2	0.370	**0.175**	0.132	0.103	0.082	0.066	0.051	0.043	0.103
3	0.526	0.374	**0.283**	**0.220**	**0.174**	0.139	0.110	0.087	**0.168**
4	**0.359**	**0.254**	**0.191**	0.149	0.118	0.092	0.076	0.062	0.149
5	**0.247**	**0.175**	0.132	0.101	0.079	0.063	0.048	0.038	0.101
6	0.000	0.000	0.000	0.000	0.000	0.000	0.000	0.000	0.000
237 K									
2	0.449	**0.209**	0.157	0.122	0.097	0.076	0.059	0.050	0.121
3	**0.352**	**0.253**	**0.190**	0.148	0.116	0.094	0.074	0.058	0.148
4	**0.248**	**0.177**	0.134	0.103	0.081	0.063	0.051	0.043	0.103
5	0.159	0.114	0.085	0.066	0.051	0.039	0.031	0.024	0.032
6	0.107	0.076	0.057	0.044	0.035	0.027	0.021	0.015	0.000
290 K									
2	0.364	**0.228**	**0.171**	0.133	0.105	0.083	0.066	0.055	0.101
3	0.479	**0.342**	**0.258**	**0.200**	0.159	0.126	0.104	0.082	**0.200**
4	0.680	0.487	0.366	**0.284**	**0.223**	**0.175**	0.148	0.116	**0.247**
5	0.150	0.107	0.080	0.062	0.049	0.037	0.030	0.024	0.062
6	0.000	0.000	0.000	0.000	0.000	0.000	0.000	0.000	0.000
348 K									
2	0.582	0.416	0.383	**0.244**	**0.194**	0.154	0.127	0.100	0.156
3	0.562	0.403	**0.302**	**0.235**	**0.187**	0.147	0.117	0.099	**0.179**
4	0.606	0.427	**0.323**	**0.251**	**0.194**	0.150	0.123	0.092	0.129
5	0.409	**0.222**	**0.167**	0.129	0.099	0.075	0.061	0.046	0.029
6	**0.320**	**0.224**	**0.172**	0.130	0.104	0.079	0.066	0.052	0.041

Table 8: *A* parameters for several threshold angles, obtained from a series of simulations at the usual state points by Equation 13. Bold: values within the experimental results (0.36 and 0.16 cP/ps). The rightmost column contains results when only the kinetically activated events are used for the calculation of the rate constant. See text.

the early phase of the reaction, up to approximately 100 fs, this angle does virtually not change. Afterwards, there is a substantial change, which is nicely correlated with the flattening of the central dihedral angle trajectory (solid line) after it has crossed the barrier at 92°.

Some individual dihedral angle trajectories

The initial downhill motion (Figure 7 phase A, both central and phenyl dihedrals involved) and the barrier crossing (primarily central dihedral involved) occur in different directions in conformation space. In other words, there is a bend between the straight lines from the *cis* peak to the *gauche* minimum and from the *gauche* minimum to the barrier saddlepoint in Figure 4. Thus, a transfer of kinetic energy is required for isomerisation, although the energy might easily reach a value above the barrier. This observation is confirmed by looking at individual trajectories, e. g. in Figure 9. Both trajectories come from the same series of simulation with equal temperature and pressure. However, the solid line shows a trajectory that leads to isomerisation, while the dashed line represents a trajectory that ends up in the *gauche* minimum. Looking at the energy trajectory of the latter, it is evident that the energy

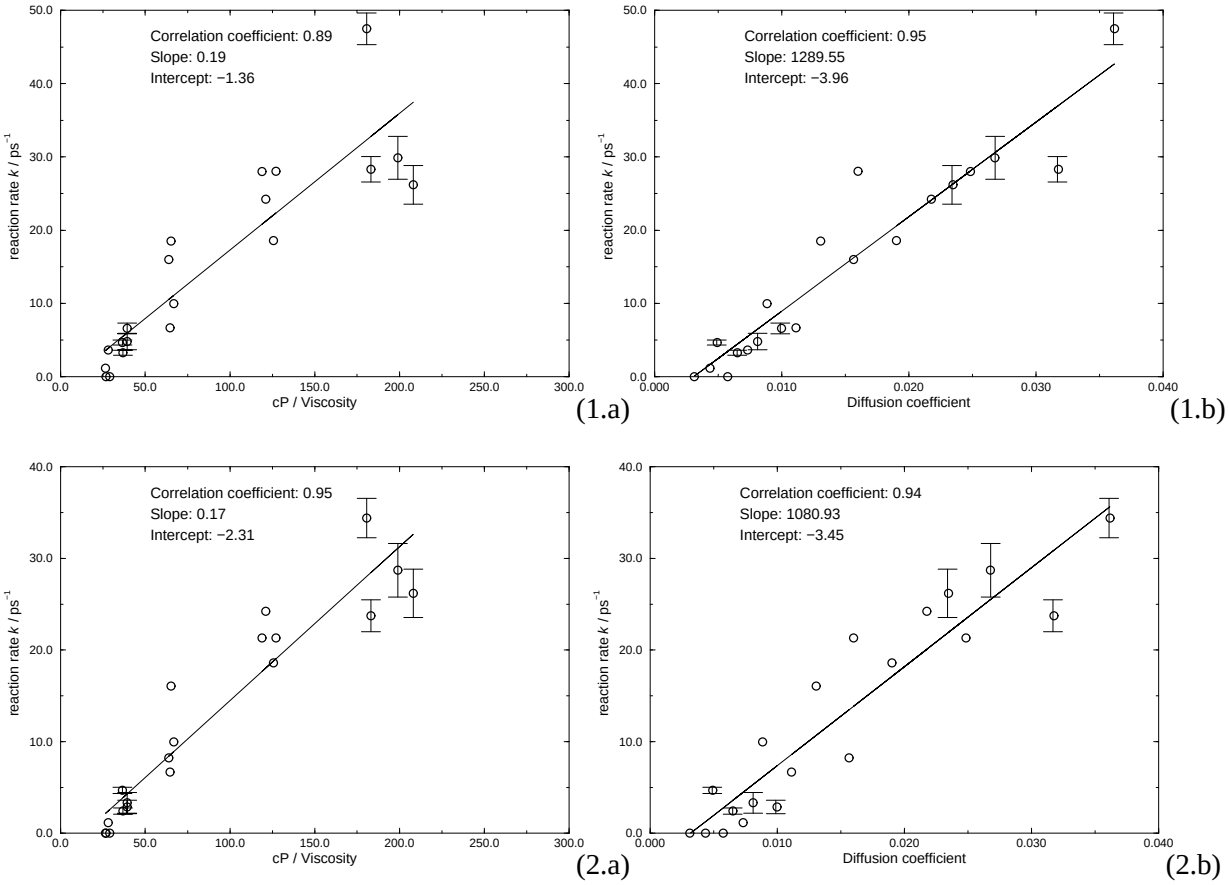

Figure 6: Linear regression of the inverse shear viscosity and the diffusion coefficient of the solvent with the reaction rate constant k. Error bars are shown for the points with estimated standard deviation from the three series of simulations (box types 2 and 5). (1) Normal rate constant, (2) Rate constant including kinetic activations only (see text), (a) Inverse viscosity, (b) Diffusion coefficient in nm^2/ps. Calculated from the 50° threshold angle. Results from the linear regression are shown as insets.

reaches approximately 45 kJ/mol, which is considerably higher than the barrier. So, from an energetic point of view, a barrier crossing would easily be possible. It does not take place because the molecule is not in the vicinity of the saddlepoint.

Looking at the other trajectory (solid line), the maximum energy (apart from the initial part) is much lower than in the first one. Nevertheless, it is comfortably above the barrier height and exhibits an isomerisation. Interesting is again that the trajectory flattens between 90° and 120° for the central dihedral angle. The major difference between the two trajectories in the first phase is the evolution of the phenyl torsion angles. While these angles are heavily distorted to nearly −30° in the trajectory without isomerisation, they are drastically quenched in the other trajectory and hardly reach −10°. This effect directs the motion of the molecule towards the saddlepoint and over to the *trans* region. A sample trajectory is shown in Figure 3 as a white line. The barrier is also clearly visible and is straight on the $r_2 = 92°$ line.

Looking at Figure 3, it is not difficult to imagine why the barrier is rarely crossed at its minimum energy point. Falling down from the initial Franck-Condon region in the lower left corner in Figure 3, the molecule keeps its reaction direction when climbing the wall on the other side of the minimum. By looking carefully at the contour lines when climbing, one realises that the driving force towards the barrier is not very strong, as the contour lines are crossed nearly perpendicularly.

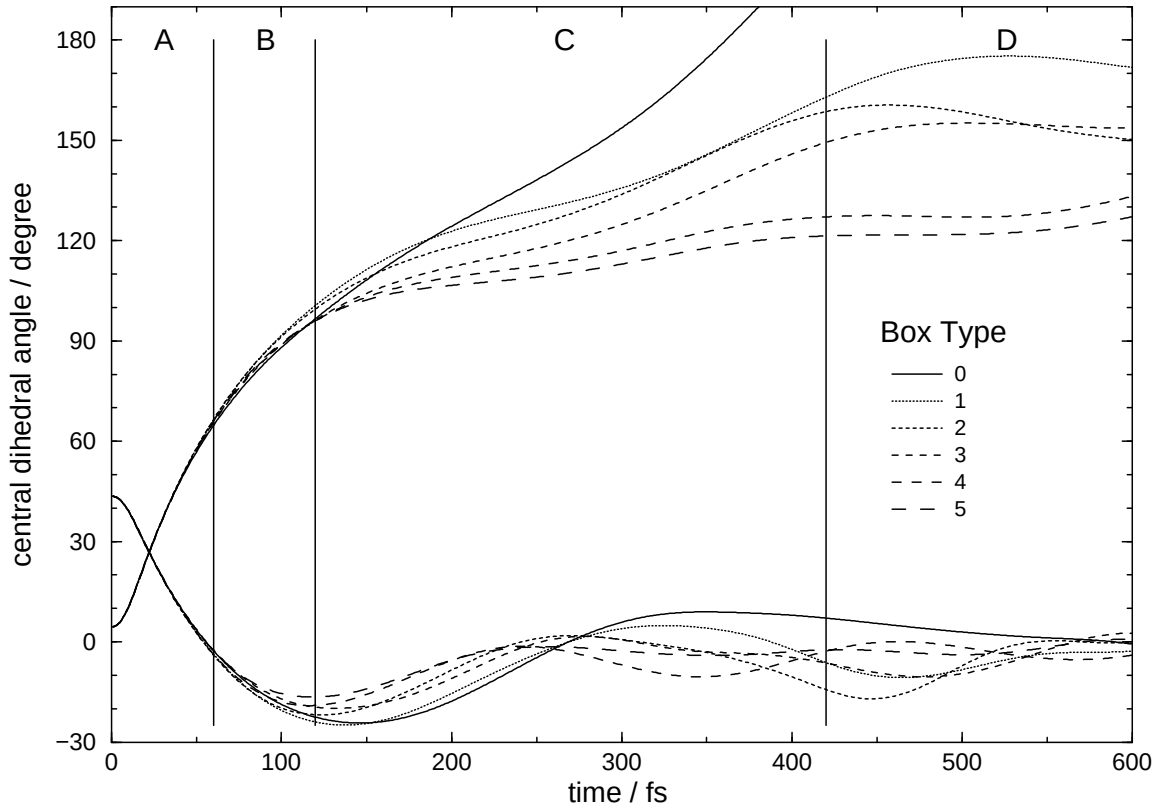

Figure 7: Averaged trajectories of simulations at 190 K that exhibit isomerisations to the *trans* minimum (Class I from Table 3).

Reason for the Barrier-Recrossings

Several trajectories exhibit barrier recrossings, i. e. the barrier is actually crossed, but the *trans* minimum is not reached, but rather the molecule is pushed back to the *gauche* region, without prior relaxation. This behaviour is shown in Figures 4 and 9. Beyond the barrier, the potential energy surface does not exhibit any back-driving gradient. Therefore, the force reverting the inertial motion of the molecule must have another source. However, the gradients of the potential energy surface along the central dihedral angle are rather small, as opposed to the gradients along the phenyl torsion angles (mind the scaling of the pictures of the potential energy surface). This is likely to have two consequences: (i) The driving force to either minimum is not very strong. This is illustrated in Figure 7. In phase C, after the barrier has been crossed, the central dihedral angle does not move as fast as in phase A, even for the vacuum trajectory. At the same time, the phenyl torsion angles change vividly (Figure 4). (ii) The force required to revert the motion of the central dihedral angle does not need to be very high.

Figure 10 shows averaged trajectories of the solute-solvent interaction potential energy for the three classes of reactions from Table 3. These classes exhibit qualitatively different behaviour. (i) The reactions which are immediately quenched in the *gauche* minimum encounter a high peak at 70 fs / 29 kJ/mol (dotted line). In this case, the solvent atoms form a strong energy wall which cannot be broken through. Thus isomerisations are not possible. (ii) The isomerisations feature a low peak at 90 fs / 9 kJ/mol (dashed line), then a basin, and a second peak at 260 fs / 13 kJ/mol. The first frictional barrier is overcome, and the first solvation shell relaxes a bit while the isomerisation continues. The second peak is overcome when the *trans* region is reached. (iii) The barrier recrossings are characterised by a broad lobe between 100 fs / 14 kJ/mol and 220 fs / 16 kJ/mol (solid line). These features are present in

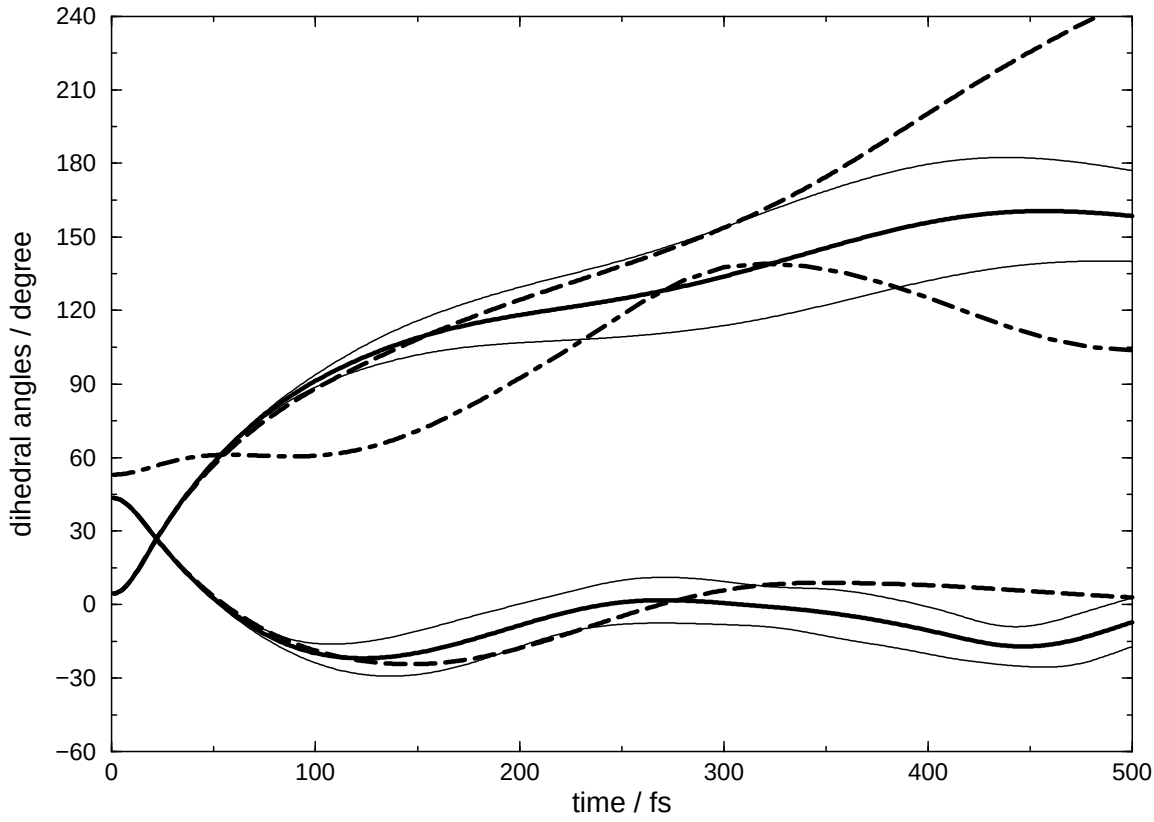

Figure 8: Averaged trajectories of simulations at 190 K that exhibit isomerisations to the *trans* minimum with 6.235 nm box size. Solid lines: central and one phenyl torsion dihedral angles, together with standard deviations. Both phenyl torsion angles are similar, but not identical. Dashed lines: Trajectory of a single simulation of the system in vacuo. As the system is simulated from a symmetric initial conformation, the two trajectories of the phenyl torsional angles coincide. Dot-dashed line: angle between the plane normals of the two phenyl rings.

the individual trajectories in a more or less pronounced manner, and are not artifacts of the averaging. The error bars on every first maximum demonstrate that the three classes of trajectories are quite well separated.

The three classes in Table 3 can also be characterised by the energy fluxes between different energy contributions. The first phase is equal for all three classes: the solute's potential energy is transformed into kinetic energy of the solvent. The second phase is different for the three classes. For the trajectories that remain in the *gauche* minimum, the solvent kinetic energy is transformed into potential energy of the solute-solvent interaction (see the high dotted peak in Figure 10). In the next phase, the energy moves mainly into the solvent. Then the energy fluxes become less clear.

In the case of a transition, the kinetic energy of the solute is mainly transformed back into intermolecular potential energy in the second phase, i. e. is used to climb the barrier. Only a small fraction flows into solute-solvent interaction potential energy: The dashed peak near 100 fs in Figure 10 is much smaller than the dotted one. After the barrier transition, there is again a peak in the solute-solvent interaction potential energy, which is overcome by slowing down the molecule's motion.

For a recrossing event, the solute's kinetic energy is distributed to all three solvent-internal, solute-solvent, and solute-internal potential energies in the second phase. Because the increase in solvent-internal and solute-solvent potential energies is slow, it is still possible for the molecule to overcome the *perp* barrier. Unlike in the other cases, the solvent-internal and solute-solvent potential energies

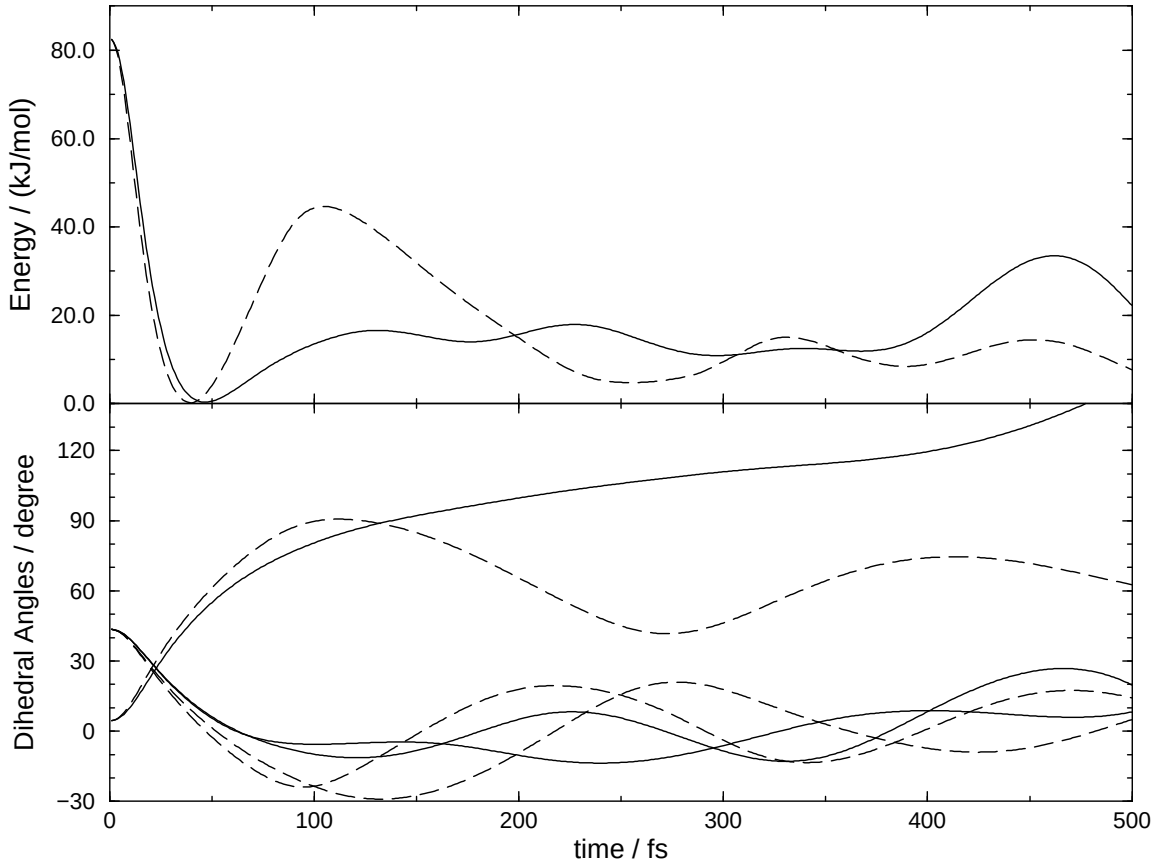

Figure 9: Examples of two individual trajectories at 290 K and 5.035 nm box size. The solid line depicts a trajectory that leads to isomerisation to the *trans* region, while the dashed line does not. Upper part: Energy trajectories; lower part: dihedral angles trajectories.

keep increasing. These high potential energies last over a relatively long time period (see the broad solid lobe between 100 and 250 fs in Figure 10) and cause the inversion of the molecule's motion and eventually make it fall back to the *gauche* region.

Figure 11 shows the effect of the first solvation shell on the molecule. One can see that the solute-only energy trajectories (thin lines) coincide with the vacuum trajectory within the first 60 fs. For the trajectories that involve barrier transitions, the similarity to the vacuum trajectory lasts up to 170 fs, which is well after the barrier has been crossed. Thus, the trajectories of the solute plus the first solvation shell (thick lines) give an appropriate representation of the solvent effect during the reaction. At first sight, it looks like the trajectories that stay in the *gauche* region have the lowest barrier (thick dotted line). This an artifact of the representation: As these trajectories do not reach the barrier, the energy remains small. It can clearly be seen that the solvent causes an increase of the barrier height, and the barrier is shifted to earlier time. To a lesser extent, the same is true for the other two reaction classes. The solute-only potential energies reach a higher level, because the barrier is indeed crossed in these cases. The solvent effect of the two classes show qualitatively different features. For the isomerisation class (dashed lines), the solvent effect causes an increase of the barrier by approximately 7 kJ/mol. In the recrossing class (solid lines), the barrier is increased by two twice this amount, and also becomes substantially broader.

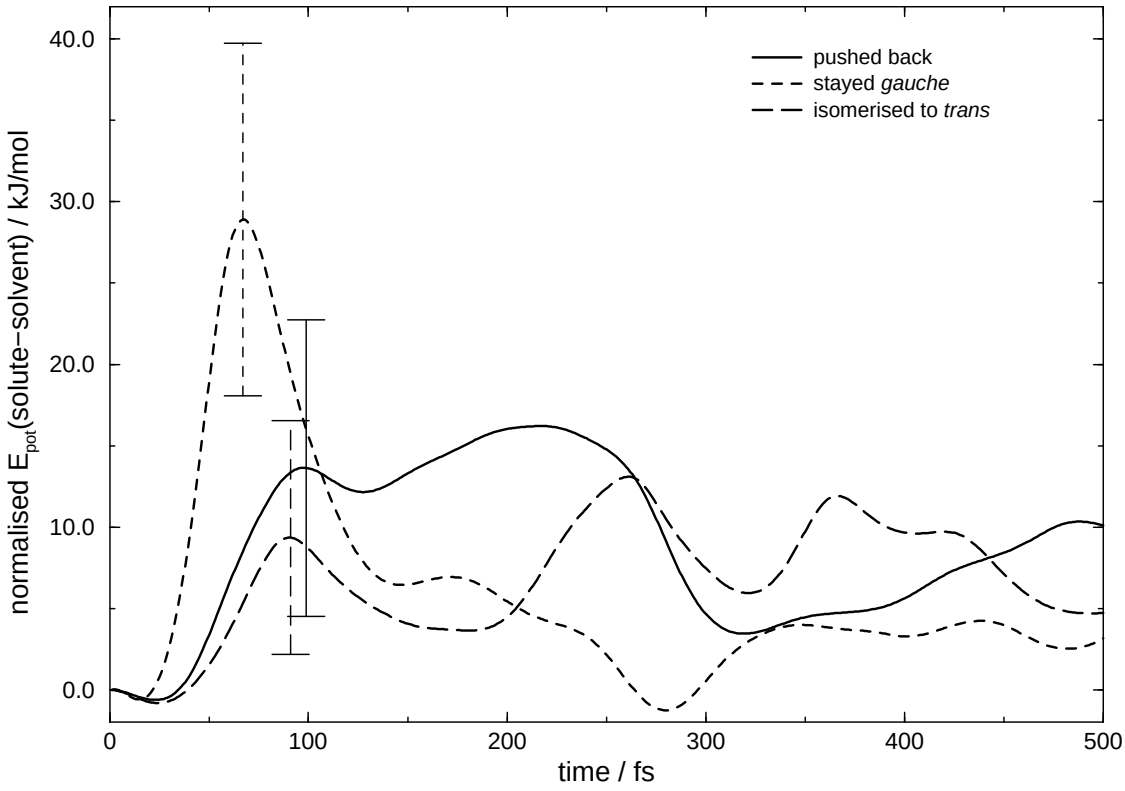

Figure 10: Averaged trajectories of the solvent-solute interaction potential energy of three classes of trajectories. The initial value of each individual trajectory has been subtracted. Average trajectories with example error bars on every first maximum are shown. An arbitrary set of 12–15 trajectories per reaction class has been averaged.

Behaviour on the Barrier

Figure 12 shows at which positions the barrier is crossed. The vast majority of dots lies in the region around -20° for both phenyl ring torsion angles. At the same time, these are nearly exclusively kinetically activated events that occur before 200 fs (circles). The later events, which are thermally activated, scatter around the barrier saddlepoint at 0° for both dihedral angles (pluses and crosses). However, some transitions still occur rather far from the saddlepoint.

Table 9 gives averages of the barrier crossing locations and averages according to increasing time window. The vast majority of the barrier encounter events occur in the two first time windows, before 200 fs. Their average energy is approximately 20 kJ/mol above the saddlepoint, and their location is 20° off the saddlepoint for both phenyl torsion angles. However, the later events are quite close to the saddlepoint in average, and their energy is approximately 4.5 kJ/mol above.

Barrier Close-ups

As a side product of our work, a detailed potential energy surface of the barrier between the *gauche* and the *trans* minimum was obtained. This barrier plays an important role in the photoisomerisation of *trans*-stilbene [6, 9–11, 36–38]. From their experimental studies, Schroeder et al. [6] draw the following conclusions: multi-dimensional barrier effects are important, and the barrier sharpens if another coordinate perpendicular to the reaction coordinate is excited. Figure 13 (c) shows a picture of this situation: While the barrier is relatively flat in its minimum, the curvature is stronger towards

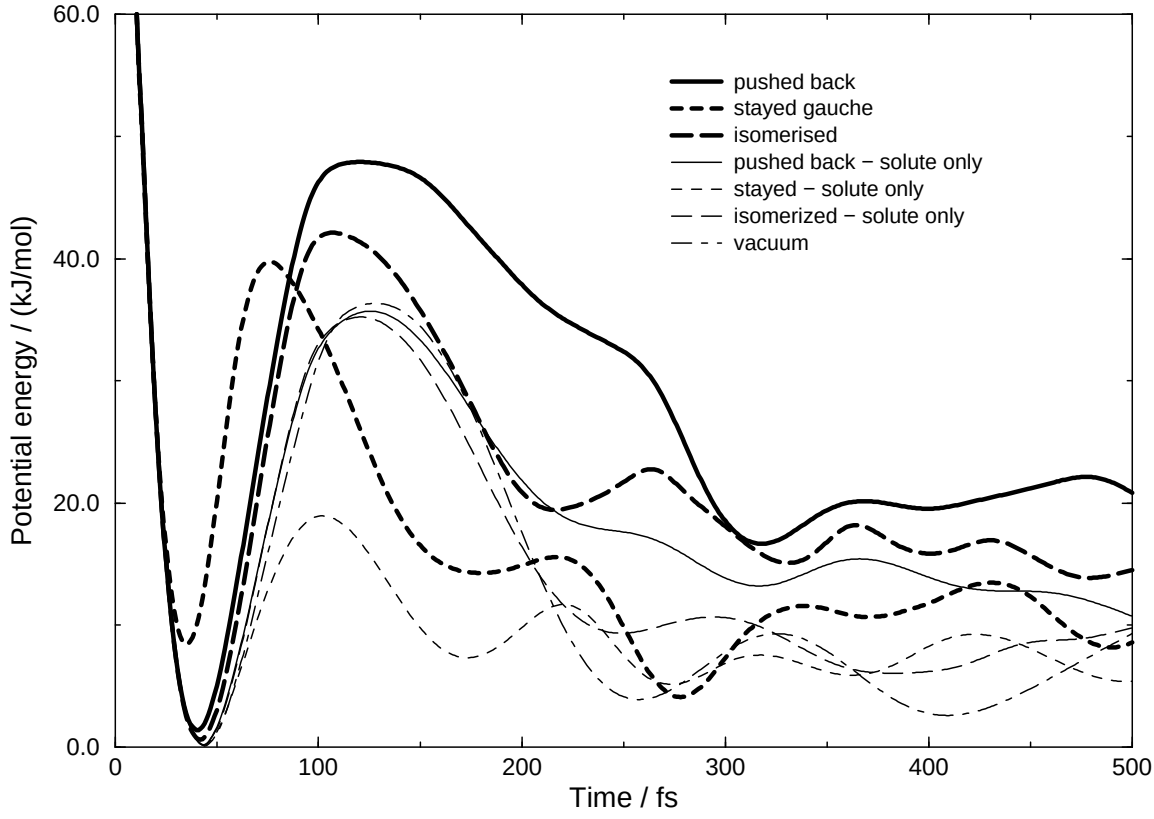

Figure 11: Potential energy trajectories of the solute only (thin lines) and together with the first solvation shell (thick lines). The same three reaction classes as in Figure 10 are shown.

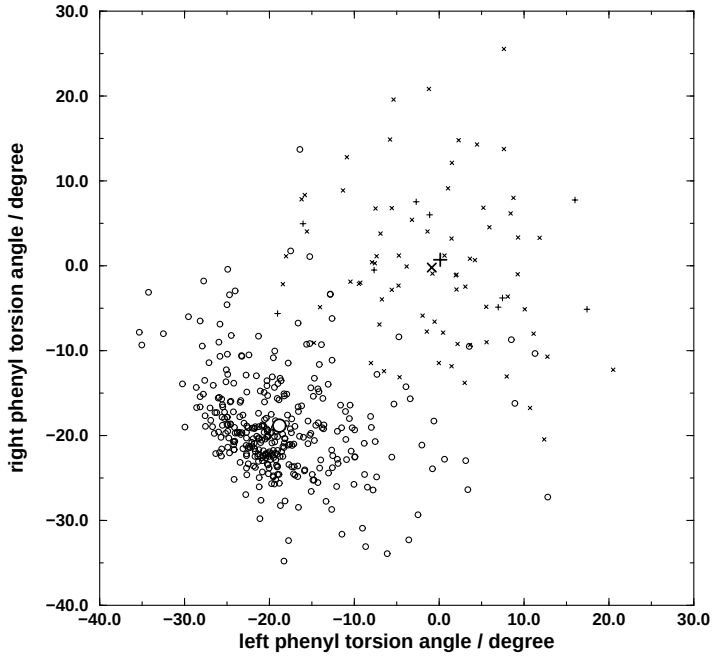

Figure 12: Cloud plot of the locations of all barrier crossings. The two axes represent the phenyl torsion angles when the central dihedral angle crosses the barrier ($r_2 = 92°$). Circles: early crossings (before 200 fs), $+$: intermediate crossings (between 200 fs and 500 fs), $\times$: late crossings (after 500 fs). The averages of the three sets are given by larger symbols.

time window / ps	averages left torsion / degrees	right torsion / degrees	energy / kJ/mol	above saddlepoint / kJ/mol	number of events
0.0-0.1	-20.0	-20.7	34.9	20.7	102
0.1-0.2	-18.3	-18.0	32.9	18.7	243
0.2-0.4	-2.6	1.7	20.2	6.0	5
0.4-0.8	3.5	0.5	18.8	4.6	18
0.8-1.6	-1.4	0.1	18.5	4.3	27
1.6-3.2	-1.7	-1.6	17.9	3.7	16
3.2-6.4	-2.8	-0.3	18.0	3.8	16

Table 9: Average barrier crossing locations with corresponding average energies, depending on the time window they occur. The vast majority of the crossings are kinetically activated. They occur before 200 fs and cross the barrier far off and much above the saddlepoint. The thermally activated events pass the barrier close to the saddlepoint in average, but still not at the saddlepoint's energy.

the walls of the barrier. However, our calculations show a different picture: The barrier gets flatter towards its walls. This finding suggests that the postulate about the special properties of the barrier, though being very elegant, is not true. In this case, the discrepancy between the experimentally observed facts and predictions by RRKM theory is not resolved satisfactorily.

However, it is likely that the multidimensionality of the barrier plays an important role in the photoisomerisation dynamics. This is certainly the case for *cis-trans* isomerisation, according to our simulated reaction trajectories. In the case of the *trans-cis* isomerisation, the starting point of the reaction is not in a high-energy region, but rather close to the shallow minimum. In this case, all reactions must be thermally activated. Our calculations suggest that even in this case the barrier crossings do not occur straight through the saddlepoint. In other words, modes perpendicular to the reaction coordinate are excited. Thus the multidimensional character of the barrier is an important aspect, as suggested by Schroeder et al. [6].

Conclusions

We have simulated the photoisomerisation of *cis*-stilbene in solution at several temperatures and pressures. The potential energy surface of the stilbene molecules is calculated by *ab initio* quantum chemistry and is represented by a finite elements grid. This representation allows a great reduction of the computational expense of the quantum chemistry. In the whole study, 4 million time steps were performed, and only 2225 explicit quantum chemical calculations were required. This gives an enhancement factor of 1800 compared to a brute force approach.

Although a rather crude model of stilbene and a low-level quantum chemical method was employed, the results are in reasonable agreement with experiment. The correlation between the reaction rate constants and the solvent shear viscosity, quantified by the parameter A from Equation 5, is correctly reproduced. However, in experiment the A parameter is independent of temperature and pressure, and the linear correlation is striking. In our studies, there is quite some spread in the A parameters dependent on both pressure and temperature, but no trends are evident. We found that the reaction rate constant correlates with similar accuracy with the diffusion coefficient of the solvent. This indicates that, for comparison with the reaction rate constant, a microscopic transport property is as suitable as a bulk property like the viscosity.

The reaction starts from a very high energy region. It is a highly non-equilibrium process. Most barrier transitions occur in one go after photoexcitation without prior relaxation to a minimum (kinetic activation), so no subsequent thermal activation is necessary. The transition energies are nearly 20

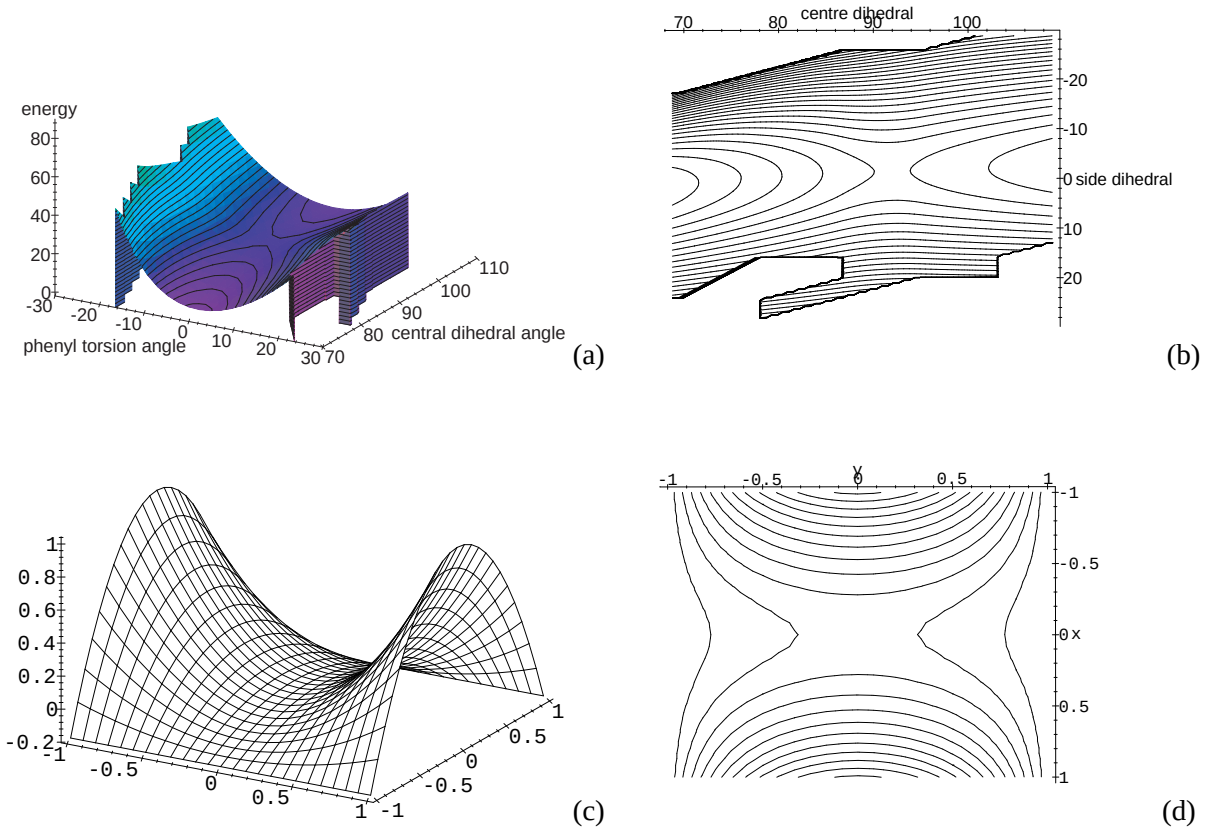

Figure 13: Barrier close-up views. (a) and (b): Barrier between the *gauche* and the *trans* minimum as obtained from our *ab initio* calculations. Distance between the contours: 2 kJ/mol. (c) and (d): Barrier shape as suggested by Schroeder et al. [6]. Distance between the contours: 0.1 arbitrary units. Both a perspective view and a contour plot are displayed for both barriers.

kJ/mol above the barrier saddlepoint. We also observed a few thermally activated barrier crossings. They average on the barrier saddlepoint, but with a considerable scatter. The picture of a minimum energy path of a reaction is inappropriate, especially for kinetically activated events.

We observed events in which the barrier was crossed, but the motion was reversed. This behaviour could be clearly attributed to a solvent effect: The solvent forms a long-lived dynamic energy barrier.

Many other authors assume a minimum on the potential energy surface of the first excited state at the 90° conformation. Our present study suggests that this state is rather at a *gauche* conformation near a 50° twist angle. This state is reached very quickly, approximately 50 fs after excitation, as suggested by Abrash et al. [5], independent of solvent friction. Similar suggestions were brought up by Myers and Mathies [35]. It is possible that the conformation probed experimentally is indeed the *gauche* conformer. This would explain the lack of spectral evolution after 100 fs. The experimentally observed exponential decay could then have sources other than a barrier near the *cis* Franck-Condon region. It might be that the process which is experimentally monitored is the barrier crossing or other sources of disappearance from the *gauche* minimum. The former involves frictional solvent effects that are nicely reproduced by our study in respect to the experimental work by Nikowa [7], while the effects important for the latter are ignored in our study.

References

[1] Marcos Dantus, Mark J. Rosker, and Ahmed H. Zewail. "Real-time femtosceond probing of "transition states" in chemical reactions". *J. Chem. Phys.*, **87**, (1987) 2395.

[2] Mark J. Rosker, Marcus Dantus, and Ahmed H. Zewail. "Femtosecond clocking of the chemical bond". *Science*, **241**, (1988) 1200.

[3] B. I. Greene and R. C. Farrow. "Subpicosecond time resolved multiphoton ionization: excited state dynamics of *cis*-stilbene under collision free conditions". *J. Chem. Phys.*, **78**, (1983) 3336–3338.

[4] Jane K. Rice and A. P. Baronavski. "Ultrafast studies of solvent effects in the isomerization of *cis*-stilbene". *J. Phys. Chem.*, **96**, (1992) 3359–3366.

[5] S. Abrash, S. Repinec, and R. M. Hochstrasser. "The viscosity dependence and reaction coordinate for isomerization of *cis*-stilbene". *J. Chem. Phys.*, **93**, (1990) 1041–1053.

[6] J. Schroeder, D. Schwarzer, J. Troe, and F. Voß. "Cluster and barrier effects in the temperature and pressure dependence of the photoisomerization of *trans*-stilbene". *J. Chem. Phys.*, **93**, (1990) 2393–2404.

[7] L. Nikowa, D. Schwarzer, and J. Troe. "Viscosity and solvent dependence of low-barrier processes: Photoisomerization of *cis*-stilbene in compressed liquid solvents". *J. Chem. Phys.*, **97**, (1992) 4827–4835.

[8] L. Nikowa, D. Schwarzer, J. Troe, and J. Schroeder. "Photoisomerization of *cis*-stilbene in compressed solvents". *Springer Ser. Chem. Phys.*, **55**, (1993) 603–605.

[9] J. Schoeder, J. Troe, and P. Vöhringer. "Pressure dependence of solvent-induced barrier shifts in the potoisomerization of *trans*-stilbene". *Chem. Phys. Lett.*, **203**, (1993) 255–260.

[10] J. Schroeder, D. Schwarzer, J. Troe, and P. Vöhringer. "From barrier crossing to barrierless relaxation dynamics. Photoisomerization of *trans*-stilbene in compressed *n*-alkanols". *Chem. Phys. Lett.*, **218**, (1994) 43–50.

[11] J. Schroeder, J. Troe, and P. Vöhringer. "Photoisomerization of *trans*-stilbene in compressed solvents: Kramers-turnover and solvent induced barrier shift". *Z. Phys. Chem.*, **188**, (1995) 287–306.

[12] David C. Todd and Graham R. Fleming. "*Cis*-stilbene isomerization: Temperature dependence and the role of mechanical friction". *J. Chem. Phys.*, **98**, (1993) 269–279.

[13] Valentin D. Vachev, John H. Frederick, Boris A. Grishanin, Victor N. Zadkov, and Nikolai I. Koroteev. "Stilbene isomerization dynamics on multidimensional potential energy surface. Molecular dynamics simulation". *Chem. Phys. Lett.*, **215**, (1993) 306–314.

[14] Valentin D. Vachev, John H. Frederick, Boris A. Grishanin, Victor N. Zadkov, and Nikolai I. Koroteev. "Quasiclassical molecular dynamics simulations of the photoisomerization of stilbene". *J. Phys. Chem.*, **99**, (1995) 5247–3497.

[15] Kim Bolton and Sture Nordholm. "A classical molecular dynamics study of the intramolecular energy transfer of model *trans*-stilbene". *Chem. Phys.*, **203**, (1996) 101–126.

[16] Gidon Gershinsky and Eli Pollak. "Theoretical study of the *trans*-stilbene isomerization reaction in ethane". *J. Chem. Phys.*, **105**, (1996) 4388–4390.

[17] G. Orlandi, P. Palmieri, and G. Poggi. “An ab initio study of the cis-trans photoisomerization of stilbene”. *J. Am. Chem. Soc*, **101**, (1979) 3492–3497.

[18] J. Troe and K.-M. Weitzel. “MNDO calculations of stilbene potential energy properties relevant for the photoisomerization dynamics”. *J. Chem. Phys.*, **88**, (1988) 7030–7039.

[19] Christian D. Berweger, Wilfred F. van Gunsteren, and Florian Müller-Plathe. “Finite element interpolation for combined classical / quantum-mechanical molecular dynamics simulations”. *J. Comput. Chem.*, **18**, (1997) 1484–1495.

[20] Christian D. Berweger, Florian Müller-Plathe, and Wilfred F. van Gunsteren. “Molecular dynamics simulation with an *ab initio* potential energy function and finite element interpolation: The photoisomerisation of *cis*-stilbene in solution”. *J. Chem. Phys.*, **108**, (1998) 8773–8781.

[21] A. Warshel and M. Levitt. “Theoretical studies of enzymic reactions: Dielectric, electrostatic and steric stabilization of the carbonium ion in the reaction of lysozyme”. *J. Mol. Biol*, **103**, (1976) 227.

[22] Martin J. Field, Paul A. Bash, and Martin Karplus. “A combined quantum mechanical and molecular mechanical potential for molecular dynamics simulations”. *J. Comput. Chem.*, **11**, (1990) 700–733.

[23] Haiyan Liu, Florian Müller-Plathe, and Wilfred F. van Gunsteren. “A molecular dynamics simulation study with a combined quantum mechanical and molecular mechanical potential energy function: Solvation effect on the conformational equilibrium of dimethoxyethane”. *J. Chem. Phys.*, **102**, (1995) 1722–1730.

[24] W. F. van Gunsteren, S. R. Billeter, A. A. Eising, P. H. Hünenberger, P. Krüger, A. E. Mark, W. R. P. Scott, and I. G. Tironi. *Biomolecular Simulation: The GROMOS96 Manual and User Guide* (vdf Hochschulverlag AG an der ETH Zürich, Zürich, 1996).

[25] M. J. Frisch, G. W. Trucks, H. B. Schlegel, P. M. W. Gill, B. G. Johnson, M. A. Robb, J. R. Cheeseman, T. Keith, G. A. Petersson, J. A. Montgomery, K. Raghavachari, M. A. Al-Laham, V. G. Zakrzewski, J. V. Ortiz, J. B. Foresman, J. Cioslowski, B. B. Stefanov, A. Nanayakkara, M. Challacombe, C. Y. Peng, P. Y. Ayala, W. Chen, M. W. Wong, J. L. Andres, E. S. Replogle, R. Gomperts, R. L. Martin, D. J. Fox, J. S. Binkley, D. J. Defrees, J. Baker, J. P. Stewart, M. Head-Gordon, C. Gonzalez, and J. A. Pople. *Gaussian 94, Revision C.3*. Gaussian, Inc., Pittsburgh PA, (1995).

[26] H. J. C. Berendsen, J. P. M. Postma, W. F. van Gunsteren, A. DiNola, and J. R. Haak. “Molecular dynamics with coupling to an external bath”. *J. Chem. Phys.*, **81**, (1984) 3684–3690.

[27] J.-P. Ryckaert, G. Ciccotti, and H. J. C. Berendsen. “Numerical integration of the cartesian equations of motion of a system with constraints: Molecular dynamics of *n*-alkanes”. *J. Comput. Phys.*, **23**, (1977) 327–341.

[28] Douglas J. Tobias and Charles L. Brooks III. “Molecular Dynamics with internal coordinate constraints”. *J. Chem. Phys.*, **89**, (1988) 5115–5127.

[29] M. Traetteberg and E. B. Frantsen. “A gas electron diffraction study of the molecular structure of *cis*-stilbene”. *J. Mol. Struct.*, **26**, (1975) 69–76.

[30] M. P. Allen and D. J. Tildesley. *Computer Simulation of Liquids* (Clarendon, Oxford, 1987).

[31] David C. Todd, John M. Jean, Sandra J. Rosenthal, Anthony J. Ruggiero, Ding Yang, and Graham R. Fleming. “Fluorescence upconversion study of *cis*-stilbene isomerization”. *J. Chem. Phys.*, **93**, (1990) 8658–8668.

[32] S. T. Repinec, R. J. Sension, and R. M. Hochstrasser. “Femtosecond studies of the photoisomerization of *cis*-stilbene in solution”. *Ber. Bunsenges. Phys. Chem.*, **95**, (1991) 248–252.

[33] Jack Saltiel. “Title unknown”. *J. Am. Chem. Soc*, **89**, (1967) 1036.

[34] Jack Saltiel. “Title unknown”. *J. Am. Chem. Soc*, **90**, (1968) 6394.

[35] Anne B. Myers and Richard A. Mathies. “Excited-state torsional dynamics of *cis*-stilbene from resonance raman intensities”. *J. Chem. Phys.*, **81**, (1984) 1552–1558.

[36] J. A. Syage, Wm. R. Lambert, P. M. Felker, A. H. Zewail, and R. M. Hochstrasser. “Picosecond excitation and *trans-cis* isomerization of stilbene in a supersonic jet: dynamics and spectra”. *Chem. Phys. Lett.*, **88**, (1982) 266–270.

[37] J. A. Syage, P. M. Felker, and A. H. Zewail. “Picosecond dynamics and photoisomerization of stilbene in supersonic beams. II. Reaction rates and potential energy surface”. *J. Chem. Phys.*, **81**, (1984) 4706–4723.

[38] David H. Waldeck. “Photoisomerization dynamics of stilbenes”. *Chem. Rev.*, **91**, (1991) 415–436.